The Astrophysical Journal, 915:68 (9pp), 2021 July 1 https://doi.org/10.3847/1538-4357/ac005b

Switchback Boundary Dissipation and Relative Age

W. M. Farrell[1], A. P. Rasca[1], R. J. MacDowall[1], J. R. Gruesbeck[1], S. D. Bale[2], and J. C. Kasper[3]
[1] NASA/Goddard Space Flight Center, Greenbelt, MD, USA
[2] University of California at Berkeley, Berkeley, CA, USA
[3] University of Michigan, Ann Arbor, MI, 051021, USA
Received 2021 March 10; revised 2021 April 29; accepted 2021 May 9; published 2021 July 7

Abstract

We examine Parker Solar Probe (PSP) magnetic field and plasma observations during its first encounter with the Sun in early 2018 November. During this perihelion time, impulsive reversals in the magnetic field, called "switchbacks," were found in the data set characterized by a quick rotation in B along with a simultaneous increase in solar wind flow. In this work, we examine the structure and morphology of 920 switchback boundaries as PSP enters and exits the structures, specifically looking for evidence of boundary degradation, dissipation, and associated ultralow frequency (ULF) magnetic wave activity. We find that boundaries with the most abrupt, step-function-like change in B_r and V_r also show little evidence of dissipation and ULF wave activity. In contrast, there is a set of boundaries that appears highly degraded with ULF magnetic activity in the vicinity of the boundary. We thus infer that the steep, step-like boundaries with little ULF activity are relatively young in comparison to the degraded boundaries. The distribution in relative ages suggests that the switchback boundary formation process is dynamic and evolving, even occurring near the PSP observation point inside of 40 R_s.

Unified Astronomy Thesaurus concepts: Solar wind (1534); Solar physics (1476); Solar magnetic flux emergence (2000); Solar magnetic fields (1503)

1. Introduction

One of the major results of the Parker Solar Probe (PSP) mission (Fox et al. 2016) is the discovery of impulsive magnetic field rotations (30° to >120°) in the near-Sun solar wind (Bale et al. 2019; Kasper et al. 2019). These rotations were accompanied by faster solar wind outflows and temperature increases (Bale et al. 2019; Kasper et al. 2019; Horbury et al. 2020; Farrell et al. 2020; Mozer et al. 2020). Individual switchback events often had dropouts in the B-field magnitude at their boundary, possibly indicative of the presence of a boundary current sheet (Farrell et al. 2020; Krasnoselskikh et al. 2020). Episodes (or clusters) of switchbacks were found between periods of quiet solar wind outflow (Bale et al. 2019), with individual switchback durations lasting tens of seconds (Horbury et al. 2020). The switchback event duration and switchback-to-switchback wait times both followed power-law distributions (Chhiber et al. 2020; Dudok de Wit et al. 2020), thus there was not a specific frequency of occurrence. The morphology of an individual switchback is thought to be cigar shaped, with elongation along the B-field direction (Horbury et al. 2020; Laker et al. 2021). During PSP's first solar encounter, the reversals were so numerous in the four-day period near the closest approach that episodes of rotation spikes occupied nearly 50% of the near-encounter interval (Horbury et al. 2020).

Figure 1 shows an individual switchback event on DOY 314 of 2018, in this case having an abrupt, step-function-like change in B_r and V_r at the PSP entry into and exit from the switchback. The time label in Figure 1(a) corresponds to the center time of the plot. Upon crossing the boundary, the B field underwent almost a complete reversal in the radial direction from −50 nT to 35 nT, while the B-field magnitude remained quasi-constant. There were two 10%–20% reductions in $|B|$ that occurred exactly at the boundary crossing, possibly in association with a boundary current (discussed previously in Krasnoselskikh et al. 2020 and Farrell et al. 2020).

Current switchback knowledge gaps include the source, evolution, and ongoing dynamics of these events, especially whether their formation process is still evolving/ongoing in situ as the switchback flows past PSP. Initial models of the switchbacks suggest they are Alfvénic magnetic fluctuations that have developed S-like kinks in their magnetic field geometry (Kasper et al. 2019; Tenerani et al. 2020), possibly forming in association with normalized wave growth during fast outward magnetoplasma expansions. Fisk & Kasper (2020) suggest that the switchbacks are a result of interchange reconnection at lower altitudes (Fisk & Schwadron 2001; Fisk 2005), with a strongly rotated B field a natural consequence of field-line disconnection from a looping magnetic topography. Similarly, Drake et al. (2021) suggested that the switchbacks are the high-altitude manifestation of flux ropes created at lower-altitude reconnection sites formed at the boundary between open and closed magnetic field topographies. In contrast to a reconnection origin, Ruffolo et al. (2020) suggest that the B-field rotations result from ongoing shear-driven dynamics between flux tubes possessing large boundary velocity differences that excite a magnetized Kelvin–Helmholtz (KH) instability. This instability creates outward propagating and evolving "roll-up" structures that initially form at a radial location just above the Alfvén critical zone. Squire et al. (2020) also suggest that the B-field rotations are an in situ process associated with the evolution of Alfvénic structures in an expanding solar wind, where the ratio of $\delta B/|B|$ is quickly increasing. These are just a few of the ideas associated with the origin of the switchbacks.

In examining sharp switchback boundaries, like those boundaries specifically targeted previously by Farrell et al. (2020), it was found that some of the most abrupt step-like switchback boundaries possessed well-defined "edges" and had very few ultralow frequency (ULF) fluctuations associated with

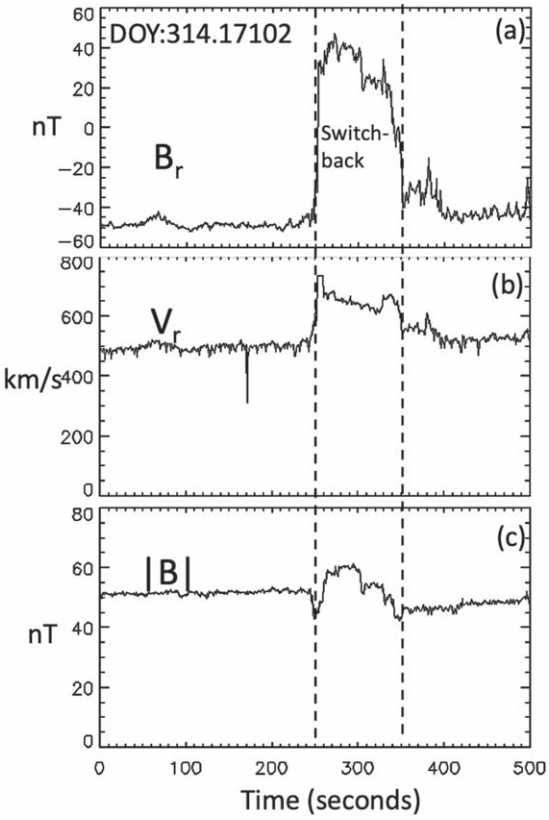

Figure 1. PSP-detected switchback event on DOY 314 of 2018.

them (like Figure 1). The ULF range is typically below 30 Hz, and we are considering waves in the range between approximately 0.07 and 1 Hz. However, there is a population of boundary crossings that have considerable ULF magnetic fluctuations associated with them, with the fluctuations occurring in a period either immediately before or after the boundary crossing. For example, three of the six switchback cases shown in Figure 7 of Farrell et al. (2020) had ULF magnetic fluctuations associated with the boundary crossings. Such cases suggest the boundary is stimulating microinstabilities or turbulence, with smaller-scale secondary instabilities forming in association with the steep boundary gradients of the larger-scale switchback structure. A possible analog might be the smaller wavelength instabilities that form in association with the sharp density boundary of spread-*F* regions in the terrestrial ionosphere (Kelley 1989). The switchback observations herein suggest a similar situation of a boundary instability leading to boundary dissipation in the form of ULF magnetic waves. The end result is an initial steep, step-like boundary that may deteriorate by becoming less step-like (smoother) in structure with the loss of its high-frequency information in the form of ULF magnetic waves.

Consequently, both the degree of steepness of the step-like functions in B_r and V_r and the presence of ULF waves could be used to determine a relative time of formation for a region of the switchback boundary. The presence of a very sharp, well-defined boundary with little ULF turbulence implies a structure that is newly formed—suggesting an in situ process still ongoing as the feature propagates past PSP. In contrast, more mature structures formed earlier may appear less step-like in their signature and have nearby ULF wave activity. In this work, we will examine a large set of switchback boundaries detected during PSP's Encounter 1 (E1) in November of 2018 using both the boundary step-function character and ULF magnetic fluctuations as a benchmark for relative age.

2. Switchback Index

The measurements for PSP's E1 were acquired via the CDAWeb (https://cdaweb.gsfc.nasa.gov/index.html/). These measurements include the FIELDS *B*-field magnitudes, $|B|$, and its components in radial-tangential-normal (RTN) coordinates along with SWEAP proton temperature and velocity moments in RTN coordinates. The data set was decimated to 1 s intervals. RTN coordinates are defined by a unit vector, *R*, in the radial direction outward from the Sun center to the spacecraft, a unit vector *T* defined by the cross-product of the solar rotation axis with *R*, and a unit vector *N* defined as an orthogonal vector to these other two vectors. A description of FIELDS' magnetometer that acquired the *B*-field data set is found in Bale et al. (2016). A description of SWEAP's particle analyzers that obtained the velocity and temperature measurements is found in Kasper et al. (2016). The measurement set thus has the variables $|B|$, B_r, B_t, B_n, T_p, $|V|$, V_r, V_t, and V_n. A set of derived quantities was also developed including the change in $|B|$, its components, and solar wind velocity and its components. We defined a derived variable δx (x is an example), where, at any instant in time t_o, the average of the x values in the 30 s after t_o was subtracted from the average of the x values in the 30 s before t_o: $\delta x(t_o) = \langle x\rangle_{\rm after} - \langle x\rangle_{\rm before}$. We thus produced a set of derived quantities, $\delta|B|$, δB_r, δB_t, δB_n, δT_p, $\delta|V|$, δV_r, δV_t, and δV_n, that is applied in the identification of step-like switchback boundaries.

As described in Farrell et al. (2020), the E1 switchback events underwent a correlation analysis, and it was found that the switchback index (SBI) that can best identify sharp switchback boundaries is $\delta B_r \cdot \delta V_r$. Specifically, as PSP enters a well-defined boundary, both δB_r and δV_r will undergo abrupt changes—with B_r changing by over 50 nT from originally negative values to positive values and V_r increasing by 100 s of km s^{-1}. In Farrell et al. (2020), those switchback boundaries that were examined had a combined change in B_r and V_r that exceeded $\delta B_r \cdot \delta V_r > 6000$ nT km s^{-1}. There were 25 such events with step-up boundaries (at PSP entry) and 28 events with step-down boundaries (at PSP exit). Step-up versus step-down boundaries can be identified via the value of $\delta B_r/|\delta B_r|$, with $+1$ indicating a step up (entry) and -1 indicating a step down (exit). In the previous work, the roughly two dozen events in each category were co-added in time via a superposed epoch analysis using the sharp boundary crossing as the common time. The co-added events revealed that, in a statistical sense, there was a precursor region found outside and adjacent to the switchback boundaries, a proton temperature increase within the switchbacks, and $|B|$ had a clear and distinct dropout in value by 7%–8% right at the boundary crossing. Not every event shows these characteristics, but enough events showed these trends to stand out in the superposed epoch analysis. The $|B|$ dropout suggests that there is a boundary current that is capable of forming a *B* field that cancels flux on either side of the boundary (nicely illustrated in Krasnoselskikh et al. 2020).

We note that there are other indices that can be used to identify switchbacks, including the z parameter, which indicates a normalized deflection of the instantaneous *B* field relative to an average value (Dudok de Wit et al. 2020). This z parameter

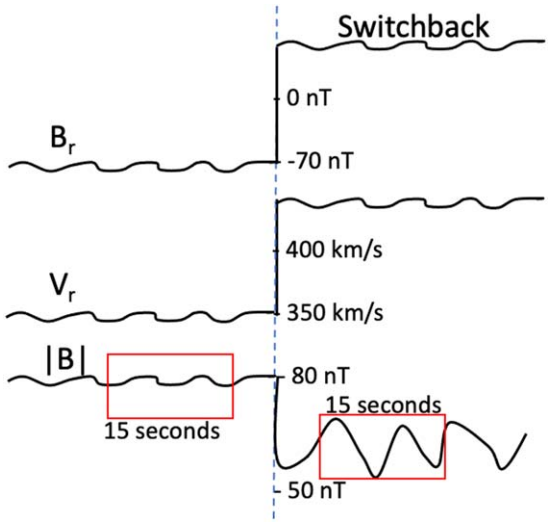

Figure 2. Illustration of the method to determine ULF fluctuations at a switchback boundary.

identifies times when the B field is undergoing a substantial rotation and nicely identifies the entire switchback period. The SBI described herein is appropriate for identifying the abrupt boundaries to the switchbacks and will have peak values at step-like boundaries (as opposed to remaining of high value throughout the entire switchback event). Thus, the two indices indeed can identify switchback events but make use of different switchback characteristics in the identification.

In this work, we extend the Farrell et al. (2020) analysis by looking at a larger number of boundary crossings (920 total) having an SBI > 1000 nT km s^{-1}. We also calculate the ULF magnetic fluctuations between 0.07–1 Hz, a variable we will call $B_{\rm ULF}$, by calculating the difference in 1 s B-field magnitude values in 15 s intervals on either side of the switchback boundary. In a 15 s window, we calculated the difference between each 1 s $|B|$ value, summed the absolute value of these differences, and divided by the number of samples (15). Note that this technique is sensitive to a fast fluctuation at a 1 s cycle (1 Hz) or any longer cycle (lower frequency) that fits in the 15 s interval ($\sim$0.07 Hz). Figure 2 is a cartoon illustrating the temporal region where the ULF wave activity was derived. We did not calculate the ULF fluctuations in a time interval $\pm$4 s about the boundary, because the dropout in $|B|$ occurring exactly at the boundary crossing can give a false enhancement of the ULF fluctuation value. We also varied the time ranges for the calculation of $B_{\rm ULF}$ (longer than 15 s to many tens of seconds) but the identification of the largest events and distribution as a function of SBI did not change substantially from the windowing applied herein. Given the measure of the ULF wave activity, we can then correlate magnetic fluctuations with SBI to determine the magnetic wave environment near the sharpest boundaries as defined by the SBI. We will first present a statistical analysis of the set of crossings and then garner further understanding by examining individual case studies.

3. Analysis of a Set of E1 Switchback Boundaries

Figure 3 shows the (a) change in $B_{\rm r}$, (b) change in $V_{\rm r}$, (c) change in proton temperature, and (d) ULF fluctuation level, $B_{\rm ULF}$, across 920 boundaries that possess an SBI > 1000 nT km s^{-1} for the E1 period extending from DOY 306 to 322 of 2018. Note that in the figure we multiply the SBI by $\delta B_{\rm r}/|\delta B_{\rm r}|$, such that negative SBI values on the left of the figure are indicative of step-down boundaries (as PSP exits the switchback) and positive SBI values on the right are step-up boundaries (as PSP enters the switchback).

As evident in Figures 3(a) and (b), there is a very strong correlation of $\delta B_{\rm r}$ and $\delta V_{\rm r}$ with SBI—as expected because the index is a direct function of $\delta B_{\rm r}$ and $\delta V_{\rm r}$. The SBI measures events with large simultaneous changes in $B_{\rm r}$ and $V_{\rm r}$ values, thus uniquely picking out step-function-like switchback boundaries in the measurement set.

Figure 3(c) shows the change in proton temperature upon crossing the boundaries, possessing the general trend that the temperature increases at entry into the switchback (SBI values > 0) and decreases upon exit of the switchback (SBI values < 0). However, we do note that in the large distribution of events, a subset of events has a temperature decrease upon switchback entry, and the temperature increases at switchback exit—just the opposite of the overall trend. These opposite events are especially apparent at low SBI values. Looking at a set of individual cases, Mozer et al. (2020) also noted that the proton temperature tended to be higher within the switchbacks.

Figure 3(d) shows the ULF magnetic fluctuation activity in the near-boundary region as a function of SBI (i.e., $B_{\rm ULF}/B$ versus SBI). There is a general trend to the data—although it is different from that of the other figures. Specifically, it is noted that the sharpest boundaries with the largest SBI (upon either entry or exit) have relatively low values of ULF magnetic wave activity. However, as the SBI moves toward intermediate positive and negative values, the number of events with large ULF wave activity increases. At low values of SBI, there are still many events with low ULF magnetic wave activity (i.e., $B_{\rm ULF}/B < 0.03$), but there is an increasing spread in the ULF event values. Notable at intermediate and low SBI values is the presence of a population of events with $B_{\rm ULF}/B > 0.1$. The dotted line in the figure places an approximate envelope over the distribution of ULF activity with the boundary crossings. A set of individual cases from this $B_{\rm ULF}/B$ versus SBI distribution will be described to garner further context.

4. Case Studies

Figure 3(d) displaying $B_{\rm ULF}/B$ versus SBI also contains the figure number (in red) of individual cases being presented herein. For example, the switchback event shown in Figure 1 has a very high positive SBI associated with PSP entry at the boundary and little ULF wave activity. This case resides on the far-right hand of the $B_{\rm ULF}/B$ versus SBI plot in Figure 3(d) (identified by the point lying near the red label "1"). For understanding, we thus selected switchbacks that possess large positive and negative SBI values found at the extreme right and left of Figure 3(d) along with those cases that possess large ULF wave fluctuation levels found near the top of Figure 3(d).

The only E1 switchback with a greater positive SBI value at PSP entry is shown in Figure 4. In this step-up boundary morphology, the change in $B_{\rm r}$ and $V_{\rm r}$ is very abrupt, with the B rotation occurring on timescales of 1–2 s. Figure 4(c) shows $|B|$ across the boundary and the presence of a sharp and distinct dropout in $|B|$ exactly at the boundary crossing (like that reported previously in Farrell et al. (2020)). However, we note that there were no obvious increases in ULF magnetic

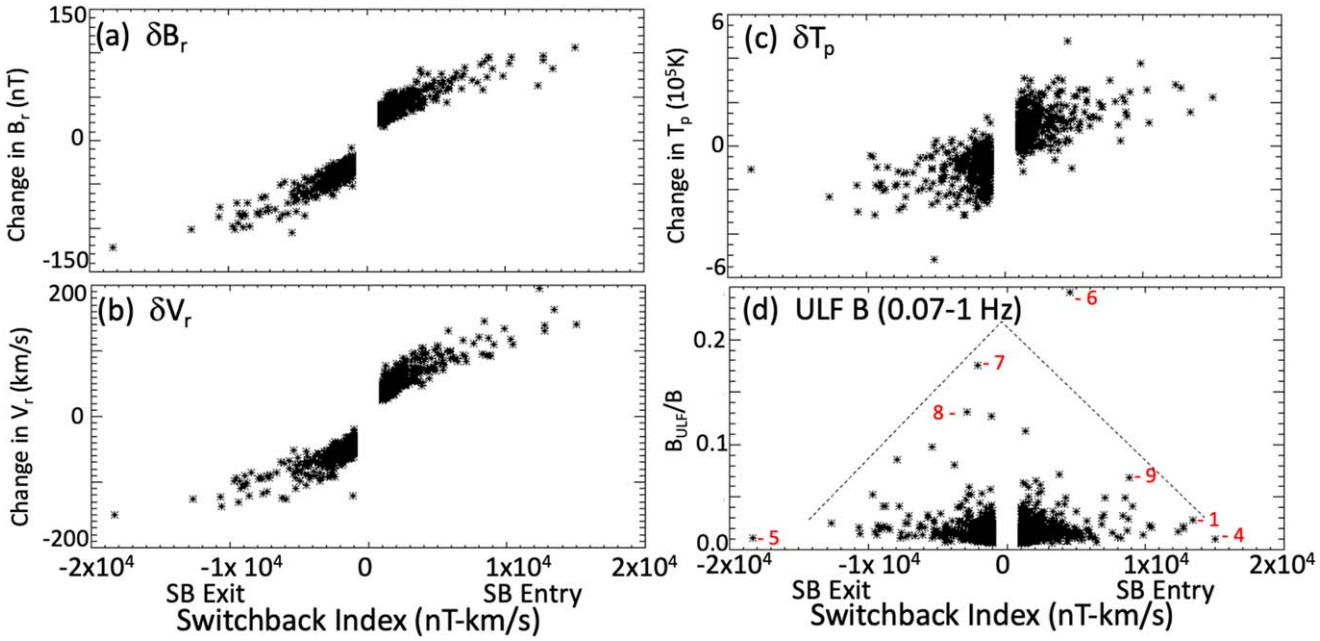

Figure 3. Shown is the (a) change in B_r, (b) change in V_r, (c) change in proton temperature, and (d) ULF fluctuation level across 920 switchback boundaries during the E1 period. In panel (d), the figure number of the individual cases associated with the data point are shown in red.

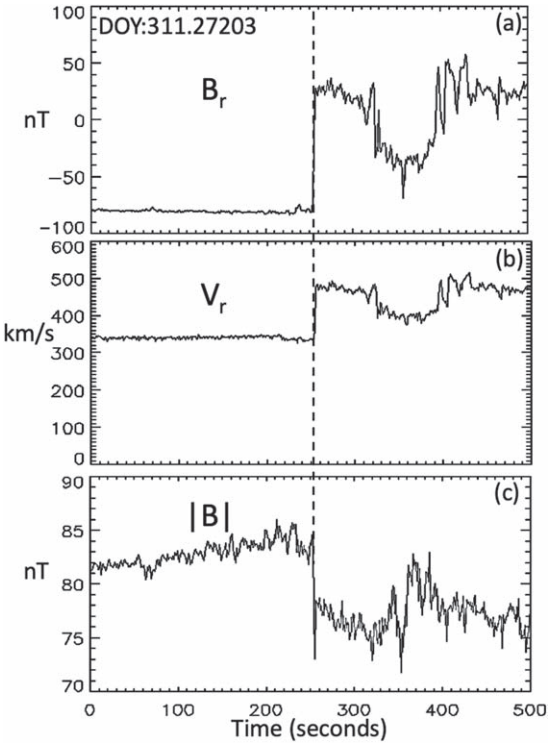

Figure 4. A PSP switchback entry on DOY 311 of 2018. The dotted line is the boundary, with the switchback on the right.

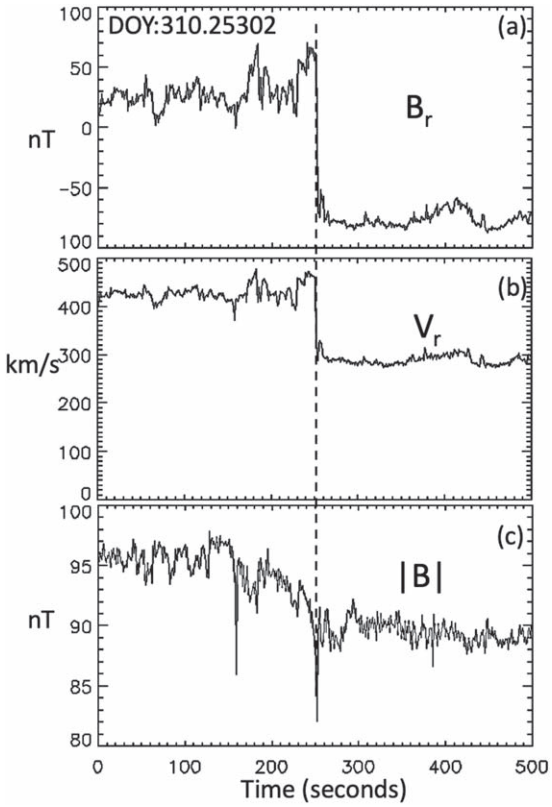

Figure 5. A PSP switchback exit on DOY 310 of 2018. The dotted line is the boundary, with the switchback on the left.

fluctuations in the tens of seconds before or after the event. Another example is shown in Figure 5, which is the case with the largest negative SBI (at PSP exit of the switchback), resulting in a step-down morphology. In Figure 3(d), this event is identified at the far left of the plot. In Figure 5, a dropout in $|B|$ is seen exactly at the boundary crossing, but the ULF fluctuation level does not increase substantially on either side of the boundary.

In contrast, Figure 6 shows a switchback event with an entry boundary that appears to be degraded/dissipated compared to the sharp step-like boundaries shown in Figures 4 and 5. Specifically, this boundary generated one of the largest ULF fluctuation signatures on our E1 set with very large $|B|$ fluctuations observed from the boundary inward into the

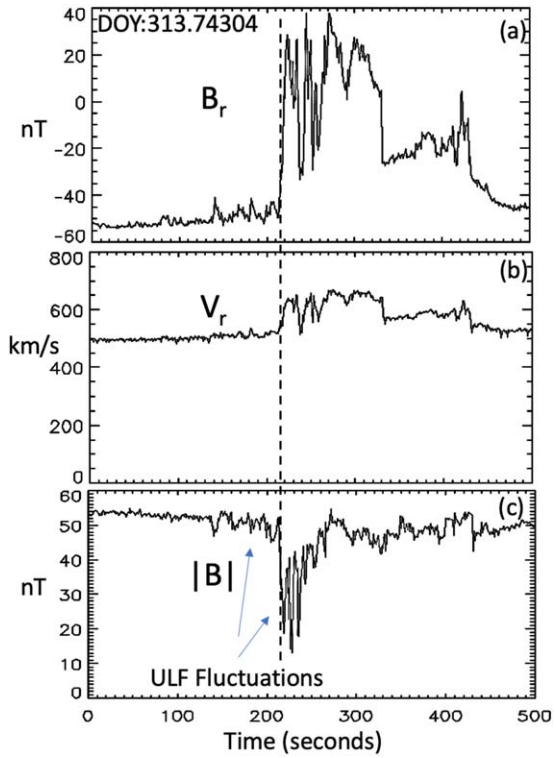

Figure 6. A PSP switchback entry on DOY 313 of 2018. The dotted line is the boundary, with the switchback on the right.

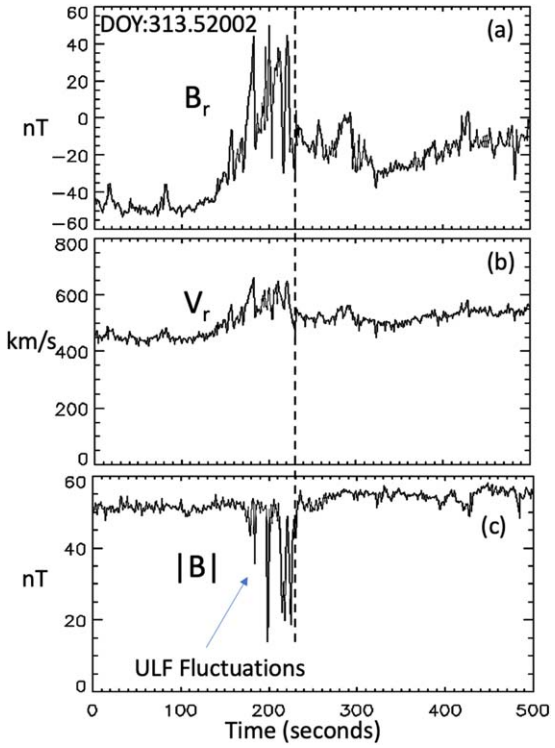

Figure 7. A PSP switchback exit on DOY 313 of 2018. The dotted line is the boundary, with the switchback on the left.

switchback. The intensity of the fluctuation near the boundary is on the order of 25 nT. This event is identified in the $B_{\rm ULF}/B$ versus SBI plot near the top of Figure 3(d). Note also the fluctuations appear in $V_{\rm r}$ as well, and the boundary as defined in $V_{\rm r}$ appears to possess a more gradual slope (in time and space) compared to those in Figures 4 and 5.

Figure 7 shows another switchback case with large ULF fluctuations on the order of 25 nT observed just adjacent to PSP's exit of the switchback. The boundary as defined in the $B_{\rm r}$ and $V_{\rm r}$ measurement really consists of a set of spikes that could be interpreted as a bundle of switchbacks rather than one large but degraded switchback. Another possible interpretation of this event is that the switchback is really the enhanced $B_{\rm r}$ and $V_{\rm r}$ levels starting from $t = 150$ s to the end of Figure 7 and that the front boundary of this extended region has an episode of enhanced fluctuations/rotations in $|B|$. In any case, the boundary is not a step-like boundary and is so clearly degraded and complex that there are multiple interpretations. Figure 8 is a third case that again shows a dissipated boundary with a gradual decrease in both $B_{\rm r}$ and $V_{\rm r}$ from $t = 0$ s to about $t = 200$ s. Enhanced ULF fluctuations near 20–30 nT levels are observed with this event as well (the event lies midway on the $B_{\rm ULF}/B$ versus SBI plot, Figure 3(d)). This kind of switchback boundary morphology is very different from the step-like cases in Figures 4 and 5.

Figure 9 is an unusual case, having a relatively large SBI value, thus possessing a sharp boundary in $B_{\rm r}$ and $V_{\rm r}$, but also having relatively large ULF magnetic fluctuations. The first few fluctuations close to the boundary are on the order of ~40 nT. In this case, $B_{\rm r}$ and $V_{\rm r}$ also do not have corresponding fluctuations in their values—the boundary appearing mostly

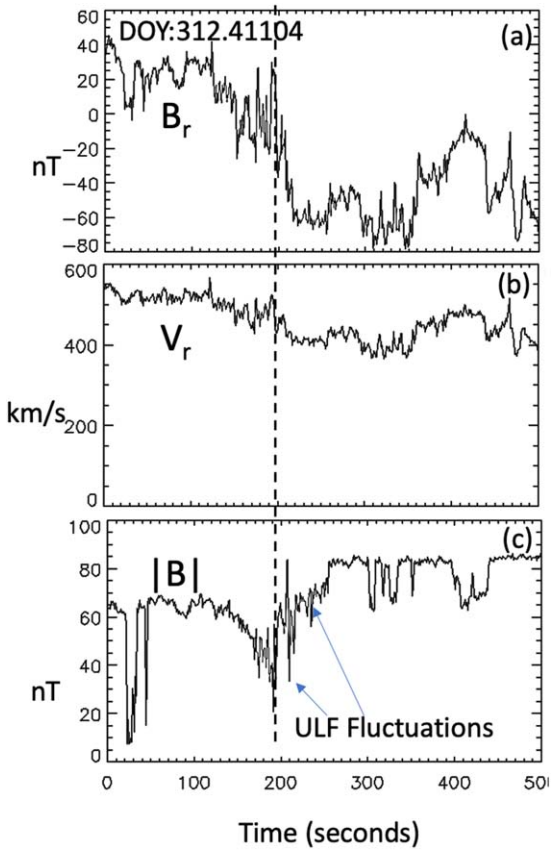

Figure 8. A PSP switchback exit on DOY 312 of 2018. The dotted line is the boundary, with the switchback on the left.

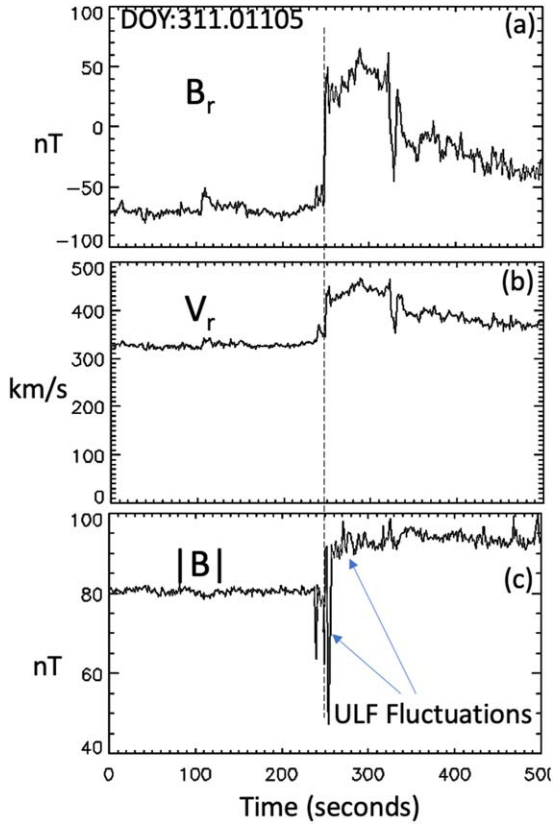

Figure 9. A PSP switchback entry on DOY 311 of 2018. The dotted line is the boundary, with the switchback on the right.

step like. This specific event is also shown in Figure 7 of Farrell et al. (2020).

5. Discussion and Conclusions

One possible (albeit nonunique) interpretation of Figure 3(d) is that the boundary ULF wave activity is an indication of the degree of dissipation of the boundary. The ULF wave activity could thus be an indication of the relative maturity of the boundary. For example, the boundaries with the largest SBI values also have relatively low ULF magnetic wave activity. This result could suggest that these very sharp boundaries have been recently formed and have not had time to become modified by the loss of high-frequency magnetic content (either by propagation or instability). In contrast, some of the boundaries with intermediate SBI values have substantial ULF wave activity, suggesting that they might have started out initially as sharp boundaries but then have undergone boundary dissipative loss via ULF magnetic wave activity. These boundaries would thus be older or more mature than the steepest boundaries with the largest SBI values. Also, as evident in Figure 3(d), mixed with these mature boundaries at intermediate SBI values is a large population of $B_{\rm ULF}/B$ values below 0.03, and we suggest that these are young boundaries with little ULF wave dissipation but have lower $\delta B_{\rm r}$ and $\delta V_{\rm r}$ across the boundary. Thus, the largest SBI-valued boundaries tend to be young (abrupt boundaries with little ULF wave dissipation) while the intermediate SBI-valued boundaries consist of a broader population in relative age ranging from young to mature. If this interpretation is correct, then the switchbacks are still evolving with a population of young boundaries just newly formed.

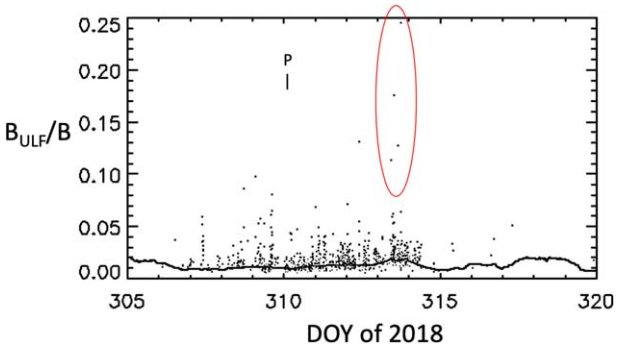

Figure 10. The ULF wave activity at each of the 920 boundaries for the encounter period (P = Perihelion).

Figure 10 shows the ULF wave activity at each of the 920 boundaries for the encounter period. The dots represent the $B_{\rm ULF}/B$ value at the individual boundary crossing (the same points in Figure 3(d)), and the solid line represents the $B_{\rm ULF}/B$ value for all 1 s data points derived in the same method as Figure 2 (15 s intervals both before and after each data point), which also have been smoothed over a day. The black curve thus represents the average $B_{\rm ULF}/B$ value throughout the encounter period. Near perihelion, early on DOY 310, the $B_{\rm ULF}/B$ values at switchback boundary crossings lie close to the average $B_{\rm ULF}/B$ value with little spread in values. However, the spread in the $B_{\rm ULF}/B$ value becomes larger at both earlier and later times. For example, there is a considerable spread in values on DOY 308–309 and again on DOY 311–312 (preceding and following perihelion, respectively). We note that on DOY 313, there are four switchback boundaries that have large $B_{\rm ULF}/B$ values above 0.1 (in the red circle). As evident in the figure, four of the top five $B_{\rm ULF}/B$ values in the entire encounter were formed on this day. As shown in Figure 1D of Bale et al. (2019), PSP's position is magnetically mapped to an equatorial coronal hole at this time, and there may be some effect on maturity when the switchback originates from a fast-streaming corona hole region. For example, we might expect relatively faster outflows that might more easily trigger boundary instabilities. However, there is also a large number of switchback boundaries with little enhanced ULF activity also originating from the hole. Thus, the advanced maturing does not appear in all switchbacks, but in only a small number of events.

The identification of switchbacks using the SBI is an automated process, where the $\mathrm{SBI} = \delta B_{\rm r} \cdot \delta V_{\rm r}$ is calculated for each 1 s data point in the entire encounter and then the local maxima in SBI values are selected as candidate boundaries. As described above, setting the threshold of 1000 km nT/s, we find that there are 920 individual boundaries identified in the E1 data set. We note there are occasions where the timing of boundaries of the same polarity (two step-up boundaries) are so close that they are likely two separate SBI identifications of a single but highly complex boundary. For example, in 2% of the events, a boundary crossing of similar polarity was encountered within 10 s of each other and 6% within 20 s of each other. Many of these anomalous boundary crossings represent an interesting class unto themselves that are worthy of future study. In many of these cases, there is a quick change in $B_{\rm r}$ and $V_{\rm r}$, then a brief decrease in their values, and then a continuation of the quick change. This effect registers as two identifications of the same boundary. Figure 11 shows an example. In

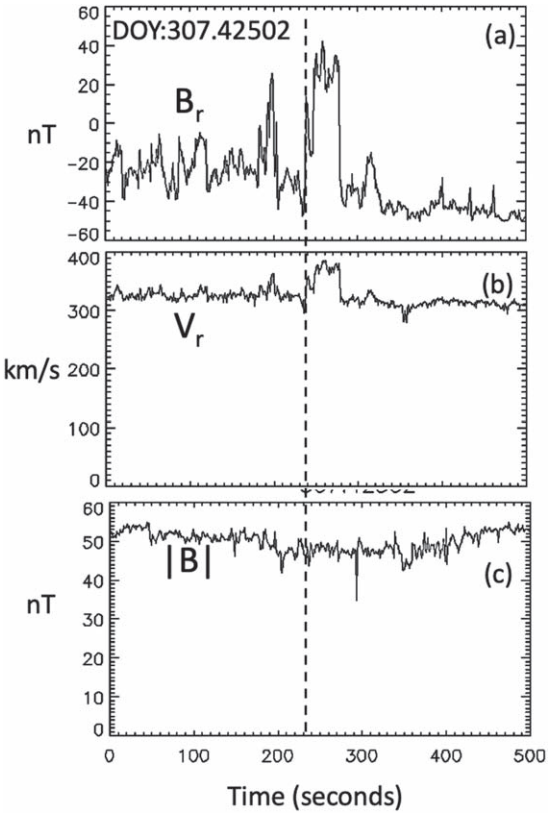

Figure 11. A PSP switchback entry on DOY 307 of 2018. The dotted line is the boundary, with the switchback on the right.

examining Figure 11 and cases like it, it may very well be that there are two separate switchback events—one smaller one preceding a larger one. Conversely, they may be one large switchback with a complex boundary that may be undergoing oscillatory displacement in time. A detailed analysis of such cases will be performed in the future.

We note that our interpretation of the switchback boundary relative age (young versus mature) based on boundary ULF activity and boundary degradation is not unique. We leave open the possibility of other ways to explain the broad range in the observed switchback boundary degradation. However, the presence of near-perfect step-function-like boundaries near perihelion (e.g., Figure 4 and 5) strongly suggests that such boundaries have undergone little dissipation, especially compared to the boundaries observed at later times and more distant regions (like those on DOY 313), consistent with being newly formed.

For example, if the switchbacks formed at lower altitudes near 10 R_s, then the features would be over 10 hours old. One thus might anticipate substantial boundary degradation on all fronts of the switchback. However, as suggested by Squire et al. (2020), the expansion process itself might be continually refreshing the boundary—creating new sharp boundaries along portions of the feature as it evolves outward. Similarly, Ruffolo et al. (2020) suggest that the shear instability process operating at sharp radial (or tangential) velocity discontinuities near the Alfvén critical zone could create a series of well-defined and evolving vortices (i.e., the switchbacks) associated with the mixing and subsequent roll-up at the interface. Their simulations show that these vortices have a broad range in boundary structure from well defined to amorphous as they evolve

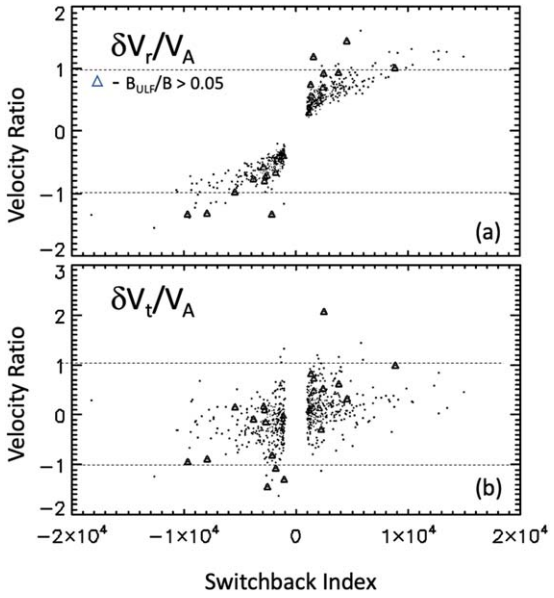

Figure 12. (a) $\delta V_r/V_A$ vs. SBI and (b) $\delta V_t/V_A$ vs. SBI for the 920 boundary crossings examined herein. Triangles represent boundaries with $B_{ULF}/B > 0.05$.

outward (see their Figure 15). Our Figure 3(d) suggests the PSP is indeed seeing a broad range of boundary structures from very sharp to amorphous/degraded, which suggests that the switchbacks are still evolving. If there is ongoing (in situ) dynamic evolution of the switchbacks, what is observed by PSP near 35–40 R_s is then not the same manifestation of the roll-up/vortex structure at locations closer to their origin.

Consider a more detailed comparison to the Ruffolo et al. (2020) model. They suggest that the overall large-scale switchback structure is a result of a magnetized KH instability that is initiated at radial distances just above the Alfvén critical zone, where the solar wind speed exceeds the Alfvén speed, $V > V_A$. They describe the general nature of the magnetized KH instability, defining the criteria for initiating the instability as (Chandrasekhar 1981) $\delta V > V_A$, where δV is the velocity shear change across an abrupt fluid velocity interface. They also note that the instability can be initiated by either an abrupt radial flow change at an interface $\delta V_r > V_A$ or a tangential flow change at an interface $\delta V_t > V_A$, the latter of which may apply close to the critical surface as the flux tubes develop a corotational component to the flow.

The simulation in Karimabadi et al. (2013) demonstrates that at the initiation of the large-scale KH instability, the roll-up structures have well defined and steep boundaries similar to our cases having high SBI and little ULF wave activity. However, as the system evolves in time, a secondary KH instability at smaller scales (and other shorter wavelength instabilities) can be excited at the steep boundary of the roll-up features (nicely illustrated in Figure 1 of Karimabadi et al. 2013). Given our data set, we can examine the development of such a secondary KH instability along the edge of the primary roll-up feature. Specifically, to determine if smaller-scale secondary KH instabilities are excited along switchback boundaries at PSP's location near 40 R_s, we apply the KH instability criteria to the 920 boundary cases examined herein.

Figure 12 shows (a) $\delta V_r/V_A$ versus SBI and (b) $\delta V_t/V_A$ versus SBI for the 920 boundary crossings examined herein. The triangles represent those mature boundaries possessing a

larger $B_{\rm ULF}/B$ exceeding 0.05. Note in panel (a) that there are many events having large SBI with flows across the interface exceeding the Alfvén speed, $|\delta V_{\rm r}|/V_{\rm A} > 1$ (on the lower left and upper right). These events might then be candidates to become unstable to a magnetic KH secondary instability. However, many of these high-speed interfaces do not possess strong signatures of ULF magnetic fluctuations (see Figures 4 and 5 as case examples). A possible conclusion to be drawn is that these boundaries are so young, so newly formed, that they have yet to commence the instability. We do find events with strong ULF fluctuation levels, $B_{\rm ULF}/B > 0.05$, but with an Alfvén Mach number at the boundary below 1. In these cases, we presume that the boundary started out unstable at lower altitudes but the energy driving the instability has been removed as the interface evolved. We also note in panel (b) that there is a set of events where the transverse velocity change across the boundary also exceeds the Alfvén speed, $|\delta V_{\rm t}| > V_{\rm A}$. In these cases, the secondary shear instability is driven by fast tangential flows over the interface. However, strong ULF magnetic fluctuations $B_{\rm ULF}/B > 0.05$ occur only in about half of these high Mach number cases. A possible conclusion is that the cases with a tangential flow exceeding a Mach number of 1 but without ULF activity are likely very young, newly formed in the context of a large-scale KH instability roll-up process, with the secondary instability expected to occur at a later time further downstream.

We note that both Lau & Liu (1980) and Miura & Pritchett (1982) have more stringent conditions on the initiation of the KH instability, including that the velocity shear has to exceed twice the Alfvén speed to become unstable $\delta {\rm V} > 2{\rm V}_{\rm A}$. However, it was also assumed in these theoretical analyses that the shear varies smoothly across the boundary and is not an abrupt discontinuous change like the cases shown herein. Future works includes comparing the cases herein to the more advanced instability criteria associated with ULF wave generation.

We also note that the wave activity in each case is not the same form. Figures 6 and 9 show a ULF wave having a quasi-coherent phase structure, suggesting there is a dominant mode being generated. In contrast, the phase is more complex in Figures 7 and 8. The ULF activity in Figure 8 has the appearance of a quasi-random phasing to the fluctuation and looks more like a turbulent structure. Figure 1 of Karimabadi et al. (2013) shows that coherent structures can devolve into more random turbulence as the instability roll-up features develop in time.

Returning to the issue of uniqueness, we note that in general there are two methods to determine ages in a sample population (of people, animals, hurricane, stars, switchbacks, etc.). One method is to follow a set of cases over time, measuring properties throughout their lifetime to determine the character of maturation. For switchbacks, this approach would require multiple measurements of the same switchback from birth at low altitudes through midlife to death—requiring multiple spacecraft all magnetically (or radially) connected to measure the properties of the switchback as it propagates outward. Obviously, this approach cannot be accomplished by PSP. The second method is to take a snapshot of a large, random population of samples and determine the ages based on morphological differences in the population. This method has an inherent nonuniqueness in that assumptions are necessary about the morphologic differences expected between young, mature, and old samples in the population. Our approach herein applies to the latter method where we examine a quasi-random population of switchback boundaries as a snapshot and use the boundary degradation and boundary ULF wave activity to infer relative age. If our underlying assumptions regarding degradation used to derive relative ages are flawed, the relative ages are not correct. Fortunately, modeling studies by Karimabadi et al. (2013), Squire et al. (2020), and Ruffolo et al. (2020) support the assumptions being applied. However, as we continue to understand the nature and character of the switchbacks, better assumptions can be built into the determination of relative switchback age (for example, better incorporation of temperature and velocity information) and future studies could provide a more accurate age.

In the future, PSP encounters will be at lower perihelion. The study herein suggests that the features observed at $35.7\,R_{\rm s}$ will become more distinct as PSP moves closer to the Sun. We might expect more abrupt step-like boundaries with higher SBI and lower ULF wave activity because the driving instability, like the magnetic KH instability (Ruffolo et al. 2020), will be in earlier stages of growth where the instability-created fluid mixing features are more distinct, possessing sharper boundaries.

In summary, we examined a set of 920 switchback boundary events as identified by a switchback index during PSP's E1 encounter, including deriving the ULF wave activity occurring in proximity to each of the boundaries. The SBI identifies those boundaries having abrupt, step-like changes in $B_{\rm r}$ and $V_{\rm r}$ across the boundary, and it was found that those boundaries with the highest SBI (most step-like) tended to have little ULF magnetic activity. However, there are also a set of boundaries with intermediate SBI values that possess clear and substantial ULF magnetic wave activity, with the boundaries appearing more disrupted and dissipated compared to the highest SBI cases. One possible interpretation is that the boundaries with the highest SBI (most step-like) are newly formed and have not undergone substantial dissipation. In contrast, those boundaries with intermediate SBI values and high ratios of $B_{\rm ULF}/B$ are more mature boundaries that may have started as step like but dissipated in time. Given that there may be a relative age to the boundaries based on ULF wave activity, we conclude that that the boundaries may be forming in situ, with those boundaries possessing the largest SBI (i.e., Figures 4 and 5) being most recently created. This interpretation is consistent with the switchbacks as still evolving fluid structures with a broad distribution of boundary types from well formed (newer) to dissipated (older) in accordance with the evolution of the structure. There may be alternate interpretations of this data set, but certainly the observations indicate that there is a clear range of degradation to the boundaries ranging from very little (e.g., Figure 5) to very substantial (e.g., Figure 8). Relative age appears to be an obvious way to interpret the degradation and dissipation findings.

We gratefully acknowledge the Parker Solar Probe project management team at Johns Hopkins University/Applied Physics Laboratory, along with the multi-institutional FIELDS and SWEAP instrument teams whose hard work and dedication created a very unique measurement set that will live on long after this exciting project is finished. This work was funded by NASA via internal WBS as part of the Solar Probe project. The data set used to create the figures can be found on NASA's CDAWWeb site (https://cdaweb.gsfc.nasa.gov/index.html/).

ORCID iDs

W. M. Farrell https://orcid.org/0000-0002-2284-7654
A. P. Rasca https://orcid.org/0000-0002-8816-3693
R. J. MacDowall https://orcid.org/0000-0003-3112-4201
S. D. Bale https://orcid.org/0000-0002-1989-3596
J. C. Kasper https://orcid.org/0000-0002-7077-930X

References

Bale, S. D., Badman, S. T., Bonnell, J. W., et al. 2019, Natur, 576, 237
Bale, S. D., Goetz, K., Harvey, P. R., et al. 2016, SSRv, 204, 49
Chandrasekhar, S. 1981, Hydrodynamic and Hydromagnetic Stability (New York: Dover)
Chhiber, R., Goldstein, M. L., Maruca, B. A., et al. 2020, ApJS, 246, 31
Drake, J. F., Agapitov, O., Swisdak, M., et al. 2021, A&A, 650, A2
Dudok de Wit, T., Krasnoselskikh, V. V., Bale, S. D., et al. 2020, ApJS, 246, 39
Farrell, W. M., MacDowall, R. J., Gruesbeck, J. R., et al. 2020, ApJS, 249, 28
Fisk, L. A. 2005, ApJ, 626, 563
Fisk, L. A., & Kasper, J. C. 2020, ApJL, 894, L4
Fisk, L. A., & Schwadron, N. A. 2001, ApJ, 560, 425
Fox, N. J., Velli, M. C., Bale, S. D., et al. 2016, SSRv, 204, 7
Horbury, T. S., Woolley, T., Laker, R., et al. 2020, ApJS, 246, 45
Karimabadi, H., Roytershteyn, V., Wan, M., et al. 2013, PhPl, 20, 012303
Kasper, J. C., Abiad, R., Austin, G., et al. 2016, SSRv, 204, 131
Kasper, J. C., Bale, S. D., Belcher, J. W., et al. 2019, Natur, 576, 228
Kelley, M. C. 1989, The Earth's Ionosphere: Plasma physics and electrodynamics (Cambridge: Academic)
Krasnoselskikh, V., Larosa, A., Agapitov, O., et al. 2020, ApJ, 893, 93
Laker, R., Horbury, T. S., Bale, S. D., et al. 2021, A&A, 650, A1
Lau, Y. Y., & Liu, C. S. 1980, PhFl, 23, 939
Miura, A., & Pritchett, P. L. 1982, JGR, 87, 7431
Mozer, F. S., Agapitov, O. V., Bale, S. D., et al. 2020, ApJS, 246, 68
Ruffolo, D., Matthaeus, W. H., Chhiber, R., et al. 2020, ApJ, 902, 94
Squire, J., Chandran, B. D. G., & Meyrand, R. 2020, ApJL, 891, L2
Tenerani, A., Velli, M., Matteini, L., et al. 2020, ApJS, 246, 32